# Hydrogen and Carbon Dioxide Adsorption with Tetra-*n*-Butyl Ammonium Semi-Clathrate Hydrates for Gas Separations

**Hiroyuki Komatsu**
Dept. of Chemistry and Chemical Engineering, Niigata University, Niigata 950-2181, Japan

**Masaki Ota, Yoshiyuki Sato, and Masaru Watanabe**
Graduate School of Engineering, Research Center of Supercritical Fluid Technology, Tohoku University, Sendai 980-8579, Japan

**Richard L. Smith Jr.**
Graduate School of Environmental Studies, Research Center of Supercritical Fluid Technology, Tohoku University, Sendai 980-8579, Japan

*DOI 10.1002/aic.14689*
*Published online December 3, 2014 in Wiley Online Library (wileyonlinelibrary.com)*

*Gas adsorption rates of $H_2$, $CO_2$, and $H_2$-$CO_2$ gas mixture ($H_2/CO_2 = 3.4$) with tetra-n-butyl ammonium salt (bromide, chloride, and fluoride) semi-clathrate hydrate particles were measured at 269 K to assess their properties for gas separation. Equilibrium gas occupancies in the S-cages of the particles were in order of (high to low) for hexagonal structure-I, tetragonal structure-I, and superlattice of cubic structure-I structures with the maximum fractional occupancy by $CO_2$ being about 40%. The $CO_2$ diffusion rate depended on the anion size of the salt, which is attributed to distortion of the S-cage that is close to the molecular size of $CO_2$. Simulations of semi-clathrate hydrate particles with theory showed that $H_2/CO_2$ selectivities could be as high as 36 (3.0 mol% TBAF) and that selectivities for an ideal membrane (3.3 mol% TBAF) could be >100 (269 K, 0.3–4.5 MPa). Semi-clathrate hydrates have wide application as separation media for gas mixtures.*  *AIChE J*, 61: 992–1003, 2015
*Keywords: separations, gas adsorption, formation kinetics, structure, anion*

## Introduction

Development of many types of renewable resources in cooperation with local communities will be important for future distributed energy systems.[1,2] The use of biomass as a renewable resource can reduce $CO_2$ emissions, but there is still the question of its application in practical systems.[3,4] Upgrading[5–7] and reforming[8,9] technologies that give biogas derived from biomass are being examined because the sources are secure, clean, and efficient. In distributed energy systems, reducing the investment cost of the upgrading or reforming equipment is important due to the small scale of the applications.[7] Raw biogas can include corrosives such as hydrogen sulfide and ammonia so that after their separation, it is still necessary to remove water and carbon dioxide.[6,10] Many adsorbents such as zeolites strongly adsorb water, so that their regeneration requires too much energy for practical use.[11] Furthermore, pressure swing adsorption (PSA) processes with adsorbents require dry gas[6] or adsorbents that do not strongly adsorb water.

As possible gas separation media, clathrate hydrates and semi-clathrate hydrates are attractive, as they are robust materials that can be used at conditions near room temperature.[12–19] Clathrate hydrates are crystalline compounds formed from $H_2O$ and guest molecules that preferentially include a guest molecule. Clathrate hydrate systems for some gas separations have been investigated along with their physical properties.[12,19–22] Quaternary ammonium salts (QAS), such as tetra-*n*-butyl ammonium bromide (TBAB), were recognized in early research as compounds that can be used to form semi-clathrate hydrates.[23] Semi-clathrate hydrates are generally more stable than clathrate hydrates according their physical properties and pressure–temperature behavior.[24] In semi-clathrate hydrates, QAS replace a small percentage of $H_2O$ molecules to form a hydrate framework with tetra-*n*-butyl ammonium cations ($TBA^+$) being included as a cation and anions ($Br^-$) substituting some number of host water molecules.[25] Semi-clathrate hydrates that can be used repeatedly and are regarded as being environmentally friendly because the included salts are involatile. The potential of semi-clathrate hydrates as gas separation media has been evaluated for a number of systems, however, their properties and characteristics are still not well known.[13,15,16,18,26–29] Factors that affect the separation characteristics of TBA salt species for mixture gases are also not known, therefore, it is difficult for the separation technology to be further advanced without new measurements or simulations.

The characteristics of semi-clathrate hydrates vary greatly according to the type of QAS that is used. Systematic

Additional Supporting Information may be found in the online version of this article.

Correspondence concerning this article should be addressed to R.L. Smith Jr at smith@scf.che.tohoku.ac.jp.

**Table 1. Description of Semi-Clathrate Hydrate Structures: Hexagonal Structure-I (HS-I), Tetragonal Structure-I (TS-I) and Superlattice of Cubic Structure-I (SCS-I)**

| Crystal Systems (abbreviation) | $N_{H_2O}(N_{ideal,H_2O})$ | $N_{TBA\ salt}$ | $N_S$ | TBA Salt | Hydration Number | $N^*_{H_2O}$ | Lattice Constants [Å] | | | Ref. |
|---|---|---|---|---|---|---|---|---|---|---|
| | | | | | | | *a* | *b* | *c* | |
| Orthorhombic (HS-I) | 76 (80) | 2 | 6 | TBAB | 38 | 76 | 21.06 | 12.643 | 12.018 | Shimada[32] |
| Tetragonal (TS-I) | 162 (172) | 5 | 10 | TBAB | 32.8 | 164 | 23.57 | | 12.3 | Davidson[25] |
| | | | | TBAC | 30.4 | 152 | 23.582 | | 12.415 | Rodionva[30] |
| | | | | TBAF | 32.8 | 164 | 23.52 | | 12.3 | Dyadin[33] |
| Cubic (SCS-I) | 344 (368) | 12 | 16 | TBAF | 29.7 | 356.8 | 24.375 | | | Komarov[34] |

Lattice constants shows are typical values for each structure and tetra-*n*-butyl ammonium (TBA) salt. There structure parameters were determined with X-ray study.[25,30,32–34]

TBAB: tetra-*n*-butyl ammonium bromide, TBAC: tetra-*n*-butyl ammonium chloride, TBAF: tetra-*n*-butyl ammonium fluoride.

$N_{ideal,H_2O}$: ideal number of water molecules per unit cell, $N_{H_2O}$: number of non-replaced water molecules as host molecule by cation and anion of TBA salt per unit cell, $N^*_{H_2O}$: reported number of water molecules per unit cell, $N_{TBA\ salt}$: number of included TBA salt molecules in semi-clathrate hydrate structure per unit cell, $N_S$: number of S-cage of semi-clathrate hydrate per unit cell.

variation of the QAS anion is the method considered in this work for studying the characteristics of the particles formed and their gas adsorption behavior. In this article, the effect of the anion ($Br^-$, $Cl^-$, and $F^-$) of the TBA salt on the adsorption characteristics of semi-clathrate hydrates for $CO_2$ and $H_2$ gases is investigated.

Typical structures of semi-clathrate hydrates are tetragonal structure-I (TS-I), hexagonal structure-I (HS-I), and superlattice of cubic structure-I (SCS-I) in the TBA salts with theoretical structures being $10(5^{12})\cdot16(5^{12}6^2)\cdot4(5^{12}6^3)\cdot172H_2O$, $3(5^{12})\cdot2(5^{12}6^2)\cdot2(5^{12}6^3)\cdot40H_2O$, and $16(5^{12})\cdot48(5^{12}6^2)\cdot368H_2O$ for TS-I, HS-I, and SCS-I, respectively.[30,31] The structures of semi-clathrate hydrates depend on the anion species and on the formation conditions of temperature and concentration of the TBA salt.[32,33] In semi-clathrate hydrates, there is the possibility that an $H_2O$ molecule can occupy the ($5^{12}$) cage (S-cage).[34] Moreover, there is strong evidence that the S-cage is of two types (a distorted cage and a regular cage) with one structure being more effective for $CO_2$ capture than the other.[35]

Investigations regarding the structure and phase equilibria of semi-clathrate hydrates have been reported,[36,37] however, studies regarding the gas adsorption rate of semi-clathrate hydrate particles are scarce. In a previous study, it was found that $H_2$ or $CO_2$ equilibrium adsorption amounts depended on TBAB semi-clathrate structures[38] and it could be realized that the control of hydrate structure and hydration number of the semi-clathrate hydrate are important issues in their practical application. In this work, our objectives were to examine three different salt anions and to determine their adsorption characteristics for $H_2$ or $CO_2$ gases for the purpose of gas separations.

TBA salts chosen for study were tetra-*n*-butyl ammonium bromide (TBAB), chloride (TBAC), and fluoride (TBAF). The effect of conditions of forming semi-clathrate hydrate on the states of the semi-clathrate hydrate structures was analyzed with differential scanning calorimetry (DSC), Raman spectroscopy and by considering the equilibrium $H_2$ adsorption amounts of the structures. Gas ($H_2$ or $CO_2$) adsorption rates in the semi-clathrate hydrate particles of unitary structure-rich phases were measured. Gas adsorption mechanisms in semi-clathrate hydrate were investigated quantitatively with a newly developed model that is referred to as multiple adsorption resistance (MAR) model.[39] For this case, two types S-cages[35] were assumed to have the same gas sorbable cage because the objective was to study the macroscopic gas adsorption. The separation potential of TBA salts semi-clathrate hydrates was estimated for $H_2$ and $CO_2$ mixture gases with the MAR model. Validity of the simulation results is demonstrated by comparison with $H_2$-$CO_2$ mixture gas adsorption measurements.

## Experimental

### *Materials*

High-purity water was obtained from Advantec Toyo Kaisha, RFD250NB with an electrical conductivity below 5.5 μS/m was used in the experiments. Helium gas (99.99%, Japan Fine Products), argon gas (99.99%, Japan Fine Products), hydrogen gas (99.99%, Japan Fine Products), carbon dioxide (99.99%, Japan Fine Products), hydrogen-carbon dioxide mixture gas ($H_2$ [99.99999%]: about 80 vol%, $CO_2$ [99.995%]: about 20 vol%, Japan Fine Products), TBAB (≥98.0%, Wako Pure Chemical Industries), TBAC (>98.0%, Tokyo Chemical Industry), and TBAF trihydrate (≥97.0%, Sigma-Aldrich) salts were used without further purification. Tetra-*n*-butyl ammonium (TBA) salts are referred to as TBAB, TBAC, and TBAF, for bromide, chloride, and fluoride compounds, respectively.

### *Hydrate preparation and characterization*

Batches of semi-clathrate hydrate particles were made by loading water (ca. 15 g) and TBA salts (TBAB, TBAC, and TBAF) into a perfluoroalkoxyethylene vessel in such a way that the concentration of TBA salts were 2.6–3.7 mol% and then the contents were weighed to a precision of 1 mg with a balance (Mettler Toledo AX504) that was followed by cooling of the solution to a predefined temperature (274–295 K) with low temperature-controlled bath (LP-50P, Nippon Medical & Chemical Ins.) while stirring with a hand-made stirring bar attachment that promoted mixing throughout the vessel.

For TBA salt (TBAB,[38] TBAC, and TBAF) semi-clathrate hydrates, the effect of the concentration of TBA salt and formation temperature on the formation structure was confirmed. The formed semi-clathrate hydrates were cooled to 253 K in a freezer for at least 6 h. The solids were crushed with a mortar and pestle at liquid nitrogen temperatures and then graded with stainless steel-type 316 sieves while being kept in the freezer at 253 K. Particle size ranges of 106–150 or 250–355 μm were used in the experiments. The formation of hydrates was confirmed with a differential scanning calorimeter (DSC-6100, SII) and a laser Raman spectrometer (NRS-5100, JASCO, Tokyo) as described in previous reports.[38] Results and discussion for DSC and Raman measurements are summarized in supporting information (Table S1, Figure S1 and S2). Table 1 summarizes the preparation

conditions and characterization of the semi-clathrate hydrates.

### *Experimental apparatus*

The experimental apparatus consisted of a hydrate formation cell and a reservoir tank.[38,39] Internal agitation was not used and was not needed due to cell geometry and procedure.[38] The reservoir tank system was designed to be separated from the equilibrium cell during the loading of the reservoir tank with gas. In the hydrate formation cell, the window (outer diameter: $\phi$ 30 mm) was held externally with an O-ring (IIR-70°, Morisei Kako [$H_2$ systems] or KEF [$CO_2$ systems]) and the inner cell was made of brass. For $CO_2$ systems, an O-ring (IIR-70°, KEF) was developed that had low $CO_2$ gas solubility. The inner volumes of the hydrate formation cell and reservoir tank were 304.7 and 26.3 $cm^3$, respectively. The cell and the tank were maintained to within $\pm$0.02 and $\pm$0.05 K, respectively. Two temperature sensors that were inserted into a hole in the cell assembly wall and into the reservoir tank had uncertainties of $\pm$29 and $\pm$78 mK, respectively. Two pressure gauges on the cell and the tank had uncertainties of $\pm$1.7 and $\pm$2.3 kPa, respectively. Detailed specifications of the apparatus, such as temperature control system, temperature sensor, and pressure gauges have been described in a previous paper.[39]

### *Experimental procedure*

The experimental procedure used to study the semi-clathrate hydrates was similar to that used in previous work.[36,37] When the hydrate formation cell and the reservoir tank were cooled to 269 K, about 4 g of the TBA salt semi-clathrate hydrate particles was loaded. As soon as the hydrate formation cell and the reservoir tank were evacuated for 5 s by a vacuum pump (Hitachi Koki, VR16L), the valve between the hydrate formation cell and the reservoir tank was closed. After the reservoir tank was sufficiently evacuated by the vacuum pump, $H_2$ gas was pressurized to about 4.3 MPa, $CO_2$ gas was pressurized to about 0.9 MPa, or $H_2$-$CO_2$ mixture gas ($H_2/CO_2 = 4$) was pressurized to about 4.9 MPa in the reservoir tank. The $CO_2$ and $H_2$-$CO_2$ mixture pressures were set to an initial $CO_2$ partial pressure of about 0.9 MPa in the adsorption experiments so as to prevent the formation of pure $CO_2$ clathrate hydrate that occurs as ice-hydrate-vapor at equilibrium conditions of 268.9 K and 0.924 MPa.[40] The initial $H_2$ pressure value (ca. 4 MPa) was set to be about four times the initial $CO_2$ pressure value (ca. 0.9 MPa) on the assumption of the theoretical reactions of the reforming of $CH_4$ and water gas shift ($CH_4 + 2H_2O \rightarrow 4H_2 + CO_2$).[8] When temperature and pressure of the reservoir tank stabilized, the gas was loaded into the formation cell over a period of about 5 s ($H_2$) or 10 s ($CO_2$ or $H_2$-$CO_2$). The analysis method was based on the pressure decay method with material balances being used in the formation cell and reservoir tank as in previous work.[39] The amount of gas loaded $n_{gas,load}$, was calculated by the difference in the gas density before and after loading of the reservoir tank (Eq. 1) with the virial EoS fit to NIST correlations.[41] The second and third virial coefficients of $H_2$ were estimated from the molar volume at temperatures of 240–300 K and at pressures of 0.05–14 MPa, and those for $CO_2$ were estimated from the saturated pressure at temperatures from 217 to 303 K. The second and third mixture virial coefficients of the virial equation of state were estimated from liquid-vapor equilibria of $H_2$-$CO_2$ systems[42–45]

$$n_{gas,load} = n_{gas,R,initial} - n_{gas,R,final} \tag{1}$$

The amount of gas in the hydrate phase was calculated from the relationships below.

Volume of vapor phase

$$V_{vapor} = \frac{n_{gas,load} M_{gas}}{\rho_{gas,vapor}(t=0)} \tag{2}$$

Moles of free gas in vapor phase

$$n_{gas,vapor}(t) = \frac{\rho_{gas,vapor}(t) V_{vapor}}{M_{gas}} \tag{3}$$

Moles of gas in hydrate phase by material balance

$$n_{gas,Hyd}(t) = n_{gas,load} - n_{gas,vapor}(t) - n_{gas,leak}(t) \tag{4}$$

where the leak rate in Eq. 4 was considered to be constant. The leak rates of $H_2$ and $CO_2$ were $(6.2 \pm 0.9) \times 10^{-4}$ mmol/h and $(1.30 \pm 0.10) \times 10^{-3}$ mmol/h, respectively, which corresponds to a pressure drop rate of 0.05–0.11 kPa/h. The experiment for the run was judged to have reached the equilibrium adsorption amount when the leak rate for the run was close to that for a system without sample according to values noted above. The leak amount of gas from the O-ring, $n_{gas,leak}(t)$ was calculated using the leak rate at the end of the experiment. The volume of hydrate phase was calculated from Eq. 5 and that of the hydrate phase was calculated from Eq. 6 using the theoretical water density in the hydrate phase (Eq. 7) as given below.

Volume of hydrate phase

$$V_{Hyd} = V_{cell} - V_{vapor} \tag{5}$$

Volume of theoretical hydrate phase

$$V_{Theor\,Hyd} = \frac{n_{H_2O,Hyd} M_{H_2O}}{\rho_{H_2O,Theor\,Hyd}} \tag{6}$$

Theoretical water density in the hydrate phase is

$$\rho_{H_2O,Theor\,Hyd} = \frac{N_{H_2O} M_{H_2O}}{(a \times b \times c) N_A} \tag{7}$$

Because pores exist in the hydrate particles,[46] the difference was corrected using porosity, $\varepsilon$, as in Eq. 8

$$V_{Hyd} = \frac{V_{Theor\,Hyd}}{1 - \varepsilon} \tag{8}$$

where $N_{H_2O}$ is the theoretical number of water molecules per unit cell. The lattice constants $a$, $b$, and $c$ were taken from the literature.[25,30,32–34] The porosity parameter was determined from Eqs. 5 and 6 according to previous work.[39] Table 1 summarizes $N_{H_2O}$ and lattice constants for each semi-clathrate hydrate. In $H_2$-$CO_2$ mixture systems, the gas composition of the vapor phase was analyzed with gas chromatography (GC; INFICON 3000 Micro Gas Chromatograph, Agilent Technologies) with a two column systems and a thermal conductivity detector. In the MolSieve 5A PLOT (10 m) backflush column system, the carrier was argon gas, injection time was 20 ms and backflush time was 15 s. In the PLOT Q (8 m) column system, the carrier was helium gas and injection time was 100 ms. In both columns, temperatures in the injector and column, and pressure of carrier gas were 323, 323 K and 172 kPa, respectively.

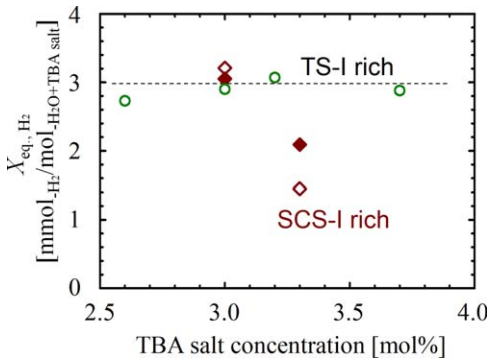


**Figure 1. Hydrogen equilibrium storage amount in TBAC or TBAF semi-clathrate hydrates ($d_p$ = 250–355 μm, $T$ = 269 K, $P_{initial}$ = 4.0 MPa).**

**Symbols show semi-clathrate hydrate formation temperatures. Green circles, TBAC, 276 K; brown diamonds, TBAF, 297 K; filled brown diamonds, TBAF, 276 K. [Color figure can be viewed in the online issue, which is available at wileyonlinelibrary.com.]**

The amount of sample gas in the cell was diluted by 1:6 by volume with Ar gas to increase its volume. Similarly, the sample gas in the tank was analyzed after dilution with Ar gas to standardize the sample gas conditions. The $H_2$ composition of sample gas in vapor phase, $y_{H_2}$ was calculated from the peak area of GC, $A_{GC,gas}$ corresponding to each gas as given by Eq. 9

$$y_{H_2} = \frac{A_{GC,H_2}/A^*_{GC,H_2}}{\frac{A_{GC,H_2}}{A^*_{GC,H_2}} + \frac{A_{GC,CO_2}}{A^*_{GC,CO_2}}} \tag{9}$$

where $A^*_{GC,gas}$ is the peak area given by GC analysis of the pure gas, which was measured for run numbers 16–20. These data reported represent the average of three values. The uncertainly of the selectively was estimated from error analysis of the $H_2$ composition.

## Results and Discussion

### *Equilibrium hydrogen storage*

Figure 1 shows $H_2$ equilibrium storage amounts in TBAC or TBAF semi-clathrate hydrates and Tables 2 and 3 (Supporting Information Table S2) summarize experimental conditions and results. The $H_2$ equilibrium storage amounts with respect to the sample (hydrate and ice), $X_{eq.,H_2}$ were calculated from Eq. 10

$$X_{eq.,H_2} = \frac{n_{eq.,H_2,Hyd}}{n_{H_2O,load} + n_{TBA\ \ salt,load}} \tag{10}$$

where, $n_{H_2O,load}$ and $n_{TBAsalt,load}$ are the amounts of $H_2O$ and TBA salt contained in the sample powder, respectively. The $X_{eq.,H_2}$ greatly depended on the semi-clathrate hydrate structure, but it did not seem to be affected by the presence of ice. The $X_{eq.,H_2}$ for the TBAC semi-clathrate hydrate systems and the 3.0 mol% TBAF semi-clathrate hydrate systems were about the same (ca. 3 $mmol_{-H_2}/mol_{-H_2O+TBA\ salt}$). The $X_{eq.,H_2}$ for 3.3 mol% TBAF semi-clathrate hydrate system values (ca. 2 $mmol_{-H_2}/mol_{-H_2O+TBAF}$) were lower those that for other semi-clathrate hydrate systems (Table 3, runs 3–10). This change in the $X_{eq.,H_2}$ implies some differences in the semi-clathrate hydrate structures.

**Table 2. Gas Adsorption Experimental Conditions for Semi-Clathrate Hydrate Particles ($T$ = 269.2 K)**

| Run | Gas | TBA Salt | Conc. (mol%) | $\Delta T$ (K) | $P_{initial}$ (MPa) | $W_{Hyd}$ (g) |
|---|---|---|---|---|---|---|
| 1[38] | $H_2$ | TBAB | 2.6 | 9 | 4.02 | 4.369 |
| 2[38] | | | 3.7 | 2 | 3.99 | 5.217 |
| 3 | | TBAC | 2.6 | 12 | 4.07 | 7.501 |
| 4 | | | 3.0 | 12 | 4.05 | 7.319 |
| 5 | | | 3.2 | 12 | 4.05 | 8.192 |
| 6 | | | 3.7 | 12 | 4.05 | 8.795 |
| 7 | | TBAF | 3.0 | 25 | 4.02 | 7.324 |
| 8 | | | 3.0 | 5 | 4.05 | 5.368 |
| 9 | | | 3.3 | 25 | 4.12 | 7.213 |
| 10 | | | 3.3 | 5 | 4.02 | 6.609 |
| 11 | $CO_2$ | TBAB | 2.6 | 9 | 0.82 | 2.389 |
| 12 | | | 3.7 | 2 | 0.84 | 2.862 |
| 13 | | TBAC | 3.2 | 12 | 0.85 | 3.380 |
| 14 | | TBAF | 3.0 | 5 | 0.84 | 4.349 |
| 15 | | | 3.3 | 5 | 0.83 | 3.789 |
| 16 | $H_2/CO_2$ = 3.4 | TBAB | 2.6 | 9 | 4.50 | 4.054 |
| 17 | | | 3.7 | 2 | 4.49 | 3.791 |
| 18 | | TBAC | 3.2 | 12 | 4.51 | 3.782 |
| 19 | | TBAF | 3.0 | 5 | 4.49 | 4.257 |
| 20 | | | 3.3 | 5 | 4.51 | 4.570 |

Particle sizes for the $H_2$ system were 250–355 μm and those for $CO_2$ system were 106–150 μm. Runs 1 and 2 are experimental conditions reported in previous work.[38]
TBAB : tetra-*n*-butyl ammonium bromide, TBAC: tetra-*n*-butyl ammonium chloride, TBAF: tetra-*n*-butyl ammonium fluoride.
$\Delta T$: degree of supercooling, $T$: temperature, $P_{initial}$: initial pressure, $W_{Hyd}$: mass (weight) of hydrate in product particles.

For TBAC semi-clathrate hydrates, the $H_2$ equilibrium storage amounts (Figure 1 and Table 3, runs 3–6) were in the order of (largest to smallest) 3.2 mol% TBAC (run 5), 3.0 mol% TBAC (run 4), 3.7 mol% TBAC (run 6), and 2.6 mol% TBAC (run 3). The reason that the $H_2$ equilibrium storage amount for 3.2 mol% TBAC semi-clathrate hydrate was the highest among the concentrations examined is due to the formation of hydrate without ice (Supporting Information Figure S1 c–f). As $H_2$ equilibrium storage amount given by in Eq. 10 is lowered by the existence of ice, some TBAC essentially had no contribution to hydrate formation due to the standardized loading amounts of the salts used. However, the $H_2$ equilibrium storage amount did not change greatly among the TBAC semi-clathrate hydrates and those values were close to those for 3.7 mol% TBAB semi-clathrate hydrate of TS-I structure (Table 3, run 2). These results are evidence that TBAC semi-clathrate hydrate had TS-I structure independent of the TBAC concentration.

For TBAF semi-clathrate hydrate in Table 3, the $H_2$ equilibrium storage amount for 3.3 mol% TBAF (run 10) was lower than half of that for 3.0 mol% TBAF (run 8). Thus, the effect of TBAF concentration on the $H_2$ equilibrium storage amount for TBAF semi-clathrate hydrates was larger than that for TBAC semi-clathrate hydrates (Figure 1 and Table 3). The difference in $H_2$ equilibrium storage amount for 3.0 mol% TBAF semi-clathrate hydrates and 3.3 mol% TBAF semi-clathrate hydrates formed near the dissociation temperature ($\Delta T$ = 5 K) was larger than that for TBAF semi-clathrate hydrates formed at 276 K ($\Delta T$ = 25 K). These results imply that semi-clathrate hydrates of different structures were formed between 3.0 mol% TBAF and 3.3 mol% TBAF, and that these two structures probably formed at the same time for the given set of conditions in which there was a large degree of supercooling ($\Delta T$). The $H_2$ equilibrium storage amount for 3.0 mol% TBAF semi-clathrate hydrate formed at $\Delta T$ equal to 5 K (Table 2, run 8) was close to that

**Table 3. Results Derived from Gas Adsorption in Semi-Clathrate Hydrates Experiments**

| Run | Gas | TBA Salt | Conc. (mol%) | $\Delta T$ (K) | $P_{final}$ (MPa) | $t_{half}$(h) | $X_{eq.,\ gas}\left(\frac{mmol_{gas}}{mol_{H_2O+TBA\ salt}}\right)$ | $\theta_{eq.,gas,\ S}$(-) | $C_{gas,\ S}$ ($\times 10^{-1}$ MPa$^{-1}$) |
|---|---|---|---|---|---|---|---|---|---|
| 1 | $H_2$ | TBAB | 2.6 | 9 | 3.90 | 0.79 | 6.67 | 0.087 | 0.238 |
| 2 | | | 3.7 | 2 | 3.93 | 0.74 | 3.21 | 0.052 | 0.136 |
| 3 | | TBAC | 2.6 | 12 | 3.97 | 0.15 | 2.73 | 0.045 | 0.117 |
| 4 | | | 3.0 | 12 | 3.94 | 0.22 | 2.90 | 0.048 | 0.126 |
| 5 | | | 3.2 | 12 | 3.93 | 0.94 | 3.07 | 0.051 | 0.134 |
| 6 | | | 3.7 | 12 | 3.93 | 0.48 | 2.88 | 0.048 | 0.126 |
| 7 | | TBAF | 3.0 | 25 | 3.91 | 0.27 | 3.05 | 0.051 | 0.134 |
| 8 | | | 3.0 | 5 | 3.97 | 0.31 | 3.21 | 0.054 | 0.140 |
| 9 | | | 3.3 | 25 | 4.04 | 0.52 | 2.09 | 0.046 | 0.118 |
| 10 | | | 3.3 | 5 | 3.97 | 0.15 | 1.45 | 0.032 | 0.081 |
| 11 | $CO_2$ | TBAB | 2.6 | 9 | 0.56 | 3.24 | 35.58 | 0.413 | 13.15 |
| 12 | | | 3.7 | 2 | 0.68 | 13.1 | 14.02 | 0.236 | 4.991 |
| 13 | | TBAC | 3.2 | 12 | 0.60 | 14.1 | 19.40 | 0.325 | 8.341 |
| 14 | | TBAF | 3.0 | 5 | 0.55 | 4.24 | 16.93 | 0.283 | 7.504 |
| 15 | | | 3.3 | 5 | 0.65 | 14.0 | 9.82 | 0.218 | 4.489 |
| | | | | | | $X_{H_2}$ | $X_{CO_2}$ | $\theta_{H_2,S}$ | $\theta_{CO_2,S}$ |
| 16 | $H_2/CO_2$ | TBAB | 2.6 | 9 | 4.21 | 2.97 | 17.68 | 0.039 | 0.230 |
| 17 | | | 3.7 | 2 | 4.40 | 1.70 | 5.63 | 0.029 | 0.095 |
| 18 | | TBAC | 3.2 | 12 | 4.40 | 1.43 | 7.07 | 0.024 | 0.118 |
| 19 | | TBAF | 3.0 | 5 | 4.35 | 1.02 | 8.02 | 0.017 | 0.133 |
| 20 | | | 3.3 | 5 | 4.44 | 0.96 | 3.82 | 0.021 | 0.085 |

Runs 1 and 2 are analysis results of raw data from previous work.[38] Time at completion of runs 16–20 was 4.0 h.
$H_2/CO_2$: $H_2 + CO_2$ mixture gas ($H_2/CO_2$=3.4). TBAB : tetra-*n*-butyl ammonium bromide, TBAC: tetra-*n*-butyl ammonium chloride, TBAF: tetra-*n*-butyl ammonium fluoride.
$P_{final}$: pressure at experimental finished, $t_{half}$: time to reach half the equilibrium gas occupancy in S-cage, $X_{gas}$: gas mole number in semi-clathrate hydrate phase by $H_2O$ and TBA salt molecules in samples, $\theta_{eq}$: equilibrium occupancy, $C_S$: Langmuir constants of gas in S-cage.

for 3.7 mol% TBAB semi-clathrate hydrate of TS-I structure (Table 3, run 2), thus, it can be concluded that the TBAF semi-clathrate hydrate (Table 3, run 8) is TS-I structure rich. The 3.3 mol% TBAF semi-clathrate hydrate formed at $\Delta T$ equal to 5 K (Table 2, run 10) for which the $H_2$ equilibrium storage amount was lowest (Table 3) is most likely SCS-I structure rich. The TS-I structure seemed to readily form for 3.0 mol% TBAF and the SCS-I structure seemed to readily form for 3.3 mol% TBAF. Detailed analyses of semi-clathrate structures are needed in the future.

### *Characteristics of gas occupancy*

Tables 2 and 3 summarize experimental conditions and results for the gas adsorption experiments. Figure 2 shows gas occupancy in the S-cages as a function of time for the TBA salt semi-clathrate hydrates for either $H_2$ or $CO_2$. The gas occupancy in the S-cage, $\theta_{gas,S}$ was calculated from Eq. 11 based on the assumption of single occupancy in the S-cage

$$\theta_{gas,S} = \frac{n_{gas,Hyd} N_{H_2O}}{n_{H_2O,load} N_S} \tag{11}$$

where $N_S$ is number of S-cages in a unit cell. When $\theta_{H_2,S}$ is 1, all S-cages are occupied with $H_2$ molecules. In Eq. 11, water molecules are assumed to not occupy the S-cage for simplicity. It should be noted, however, that different occupancies for $H_2O$ molecules have been reported for the SCS-I structure of the TBAF semi-clathrate hydrate.[33,34] This point is considered in a later section. Gas adsorption rates for semi-clathrate hydrates were assessed by the time required to reach half the equilibrium gas occupancy in the S-cage, $t_{half}$. A low $t_{half}$ value means that the adsorption rate is high and that adsorption occurs fast. The $t_{half}$ for $H_2$ systems (Table 3) were in order of (low to high) 3.3 mol% TBAF (run 10), 3.0 mol% TBAF (run 8), 3.7 mol% TBAB (run 2), 2.6 mol% TBAB (run 1), and 3.2 mol% TBAC (run 5). The $t_{half}$ for $H_2$ systems were influenced more by the anion of the TBA salt than the structure of the semi-clathrate hydrate and were in order of (shortest to longest) TBAF, TBAB, and TBAC.

The $t_{half}$ for $CO_2$ systems (Table 3) were in order of (low to high) 2.6 mol% TBAB, (run 11), 3.0 mol% TBAF (run 14), 3.7 mol% TBAB (run 12), 3.3 mol% TBAF (run 15), and 3.2 mol% TBAC (run 13). The $t_{half}$ for $CO_2$ systems depended not only on the anion of the TBA salt but also on the semi-clathrate hydrate structures. Considering the TBA anion and clathrate structure, the $t_{half}$ for $CO_2$ systems were in order of (low to high) TBA salt (TBAF, TBAB, and TBAC) and semi-clathrate hydrate structure (HS-I, TS-I, and SCS-I). The effect of the TBA anion on $t_{half}$ for $CO_2$ systems corresponded to that for $H_2$ systems. This implies that the area of the crystal grain boundary, $A_{gb}$ for the semi-clathrate hydrates increases in order of $A_{gb,TBAF} > A_{gb,TBAB} > A_{gb,TBAC}$. In fact, TBAF semi-clathrate hydrates could be easily crushed when the hydrate particles were prepared (Section Hydrate preparation and characterization). The effect of clathrate structure on $t_{half}$ for $CO_2$ systems was in correspondence with the hydration number (Table 1). The structure for low hydration numbers of TBA salts ($N_{H_2O}/N_{TBAsalt}$, Table 1) has a high ratio of anion to $H_2O$ molecules as host molecule. This means that the anion in the host framework probably inhibited inclusion of the gas molecule into the S-cage of the semi-clathrate hydrate. The volume of the distorted S-cages near the anion is smaller than that of regular S-cages[35] because the anion radius[47] is larger than that of water.[48] Therefore, the dependence of the $CO_2$ adsorption rate on semi-clathrate hydrate structure

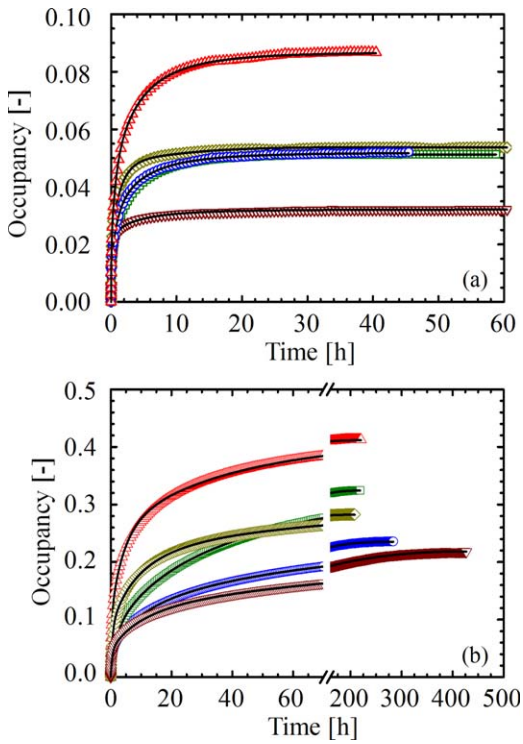


**Figure 2. Experimental and correlation results of $H_2$ or $CO_2$ occupancy as a function of time in S-cages of semi-clathrate hydrates at 269 K with multiple adsorption resistant (MAR) model.[39]**

**(a) $H_2$ adsorption systems ($d_p$ = 250–355 μm, $P_{initial}$ = 4.0 MPa). (b) $CO_2$ adsorption systems ($d_p$ = 106–150 μm, $P_{initial}$ = 0.8 MPa). Continuous lines are correlation results. Symbols show TBA salt and structure of semi-clathrate hydrate. Symbols: red up-pointing triangles, 2.6 mol% TBAB (HS-I); blue circles, 3.7 mol% TBAB (TS-I); green squares, 3.2 mol% TBAC (TS-I); olive diamonds, 3.0 mol% TBAF (TS-I); brown down-pointing triangles, 3.3 mol% TBAF (SCS-I). [Color figure can be viewed in the online issue, which is available at wileyonlinelibrary.com.]**

implies that the anion as host molecule physically inhibits $CO_2$ adsorption due to the $CO_2$ molecular size being close to the S-cage size. Especially for the TS-I structure, the $t_{half}$ for the TBAF semi-clathrate hydrate was significantly shorter than that for the TBAB and TBAC semi-clathrate hydrate because the ionic radius of $F^-$ (1.71 Å) is much smaller than that of $Cl^-$ (2.23 Å) and $Br^-$ (2.35 Å).[47]

The $H_2$ equilibrium occupancies in the S-cage, $\theta_{eq.,H_2,S}$ (Table 3) were in order of (high to low) for the semi-clathrate hydrates: 2.6 mol% TBAB (run 1), 3.0 mol% TBAF (run 8), 3.7 mol% TBAB (run 2), 3.2 mol% TBAC (run 5), and 3.3 mol% TBAF (run 10). The effect of the anion on the $\theta_{eq.,H_2,S}$ for TS-I structure (Table 3, runs 8, 2, and 5) was small but seemed to correspond to the size of the unit cell for TS-I structure (Table 1), as the $\theta_{S,H_2,eq}$ increased as the size of unit cell decreased. Thus, this result implies that van der Waals interactions between $H_2$ and $H_2O$ increase as the size of the S-cage becomes smaller. Conversely, the $\theta_{eq.,H_2,S}$ seemed to be more strongly influenced by the semi-clathrate hydrate structure (Table 3, runs 1, 5, and 10). trend implies that the S-cage was occupied by $H_2O$ molecules, because the occupancy of $H_2$ decreases with the introduction of other guest molecules according to Eq. 12

$$\theta_{eq.,H_2,S} = \frac{C^*_{H_2,S} f_{H_2}}{1 + C^*_{H_2,S} f_{H_2}} \left(1 - \theta_{eq.,other,S}\right) \tag{12}$$

where $C^*_{H_2,S}$ and $f$ are the actual Langmuir constant and fugacity, respectively. The occupancy of $H_2O$ seemed to depend on the number of anions of TBA salt as host molecule irrespective of the anion species of the TBA salt. For the case of occupied $H_2O$ as a guest molecule, the $\theta_{eq.,H_2,S}$ varies slightly because the $\theta_{eq.,H_2,S}$ calculated from Eq. 11 changes from $N_{H_2O}$ to $N^*_{H_2O}$. The $C^*_{H_2,S}$ was calculated from Eqs. 13 and 14 by considering the number of $H_2O$ molecules occupied in the S-cage per unit cell, $N_{Occ,H_2O}$ as follows

$$\theta^*_{eq.,H_2,S} = \frac{n_{eq.,H_2,Hyd}\left(N_{H_2O} + N_{Occ,H_2O}\right)}{n_{H_2O,load}\left(N_S - N_{Occ,H_2O}\right)} \tag{13}$$

$$C^*_{H_2,S} = \frac{\theta^*_{eq.,H_2,S}}{f_{H_2}\left(1 - \theta^*_{eq.,H_2,S}\right)} \tag{14}$$

where $\theta^*_{eq.,H_2,S}$ is the equilibrium occupancy of $H_2$ in the S-cage nonoccupied with $H_2O$. The $C^*_{H_2,S}$ was assumed to be equal to that for clathrate hydrates of sII structure, because the effect of distortion of the S-cage on $C^*_{H_2,S}$ is small in the sII structure due to the small molecular size of $H_2$.[39] From the measurements in this work, the Langmuir constant for $H_2$ in the S-cage for sII structure, $C^*_{H_2,S}$ was 0.04 $MPa^{-1}$ at 269 K,[39] thus, $\theta^*_{eq.,H_2,S}$ was 0.14 at 4 MPa. The $N_{Occ,H_2O}$ was estimated with the $\theta^*_{eq.,H_2,S}$, structure parameters ($N_{H_2O}$ and $N_S$) and experimental results ($n_{H_2O,load}$ and $n_{eq.,H_2,Hyd}$) in Eq. 13. The $N_{Occ,H_2O}$ for HS-I, TS-,I and SCS-I structures were taken to be 2.1, 6.0, and 12.2, respectively. These values correspond to the number of included TBA salt molecules per unit cell, $N_{TBAsalt}$ (Table 1) and implies that the number of included $H_2O$ molecules are strongly related to the number of included TBA salt species. In these results, the occupancy of $H_2O$ molecules in the S-cage were about 0.35, 0.6, and 0.76 for HS-I, TS-I, and SCS-I structures, respectively. Komarov et al. reported that the occupancy of $H_2O$ molecules in the S-cage was 0.8 for the SCS-I structure of TBAF semi-clathrate hydrate,[34] so that results in this work are in accordance with the literature.[34] From these results, it is possible for the gas adsorption capacities to be increased if the occupancy of $H_2O$ molecules can be inhibited.

The $CO_2$ equilibrium occupancy in the S-cage, $\theta_{S,CO_2,eq}$ for semi-clathrate hydrates (Table 3) were in order of (high to low) 2.6 mol% TBAB (run 11), 3.2 mol% TBAC (run 13), 3.0 mol% TBAF (run 14), 3.7 mol% TBAB (run 12), and 3.3 mol% TBAF (run 15). The $\theta_{eq.,CO_2,S}$ depended not only on the structure but also on the anion of the TBA salt in contrast to the $H_2$ systems. The $\theta_{eq.,CO_2,S}$for TBAC semi-clathrate hydrate (Run 13) was highest among TS-I structures (runs 12–15) regardless of the order of ion radii ($F^-$: 1.71 Å, $Cl^-$: 2.23 Å, and $Br^-$: 2.35 Å).[47] In TBAB semi-clathrate hydrate, the occupancy of $CO_2$ molecules in the distorted S-cages is higher than that in the regular S-cage.[35] It seems likely that the size of the distorted S-cage of TBAC semi-clathrate hydrate is optimal for the $CO_2$ molecule.

### *Analysis of gas adsorption behavior with kinetic model*

The MAR model described in a previous work[39] was applied to results in this work. Figure S3 (Supporting Information) shows the MAR model and its fitting parameters. The MAR model assumes that the hydrate particle consists of a delocalized gas-adsorbed outer shell and a localized

**Table 4. Correlation Results in Terms of the Average Relative Deviation (ARD) for Gas Adsorption Rates with the MAR Model[39] for Semi-Clathrate Hydrate Particles Formed from Tetra-*n*-Butyl Ammonium Bromide (TBAB) Tetra-*n*-Butyl Ammonium Chloride (TBAC) and Tetra-*n*-Butyl Ammonium Fluoride (TBAF) at Various Degrees of Supercooling, $\Delta T$**

| Run | Gas | TBA Salt | Conc. (mol%) | Struc.[a] | $\Delta T$ (K) | $L$(μm) | $K_a$ ($\times 10^{-4}$ s$^{-1}$) | $k_c$ ($\times 10^{-9}$ ms$^{-1}$) | $D_a$ ($\times 10^{-13}$ m$^2$s$^{-1}$) | ARD(%) |
|---|---|---|---|---|---|---|---|---|---|---|
| 1 | $H_2$ | TBAB | 2.6 | HS-I | 9 | 28.2 | 9.116 | 34.89 | 15.76 | 0.69 |
| 2 | | | 3.7 | TS-I | 2 | 33.2 | 4.094 | 52.34 | 5.127 | 1.74 |
| 3 | | TBAC | 2.6 | TS-I | 12 | 38.1 | 14.60 | 285.6 | 12.18 | 6.05 |
| 4 | | | 3.0 | TS-I | 12 | 42.9 | 7.756 | 104.2 | 19.59 | 3.07 |
| 5 | | | 3.2 | TS-I | 12 | 20.0 | 7.630 | 87.55 | 1.934 | 2.17 |
| 6 | | | 3.7 | TS-I | 12 | 27.9 | 5.656 | 145.0 | 6.949 | 7.02 |
| 8 | | TBAF | 3.0 | TS-I | 5 | 78.2 | 2.560 | 10.89 | 20.03 | 1.47 |
| 10 | | | 3.3 | SCS-I | 5 | 56.1 | 5.000 | 60.81 | 18.96 | 1.98 |
| 11 | $CO_2$ | TBAB | 2.6 | HS-I | 9 | 10.7 | 35.09 | 0.706 | 0.0238 | 1.58 |
| 12 | | | 3.7 | TS-I | 2 | 5.11 | 6.170 | 1.642 | 0.0073 | 1.83 |
| 13 | | TBAC | 3.2 | TS-I | 12 | 3.70 | 3.445 | 2.313 | 0.0111 | 2.49 |
| 14 | | TBAF | 3.0 | TS-I | 5 | 11.4 | 10.59 | 1.264 | 0.0122 | 1.42 |
| 15 | | | 3.3 | SCS-I | 5 | 6.91 | 5.907 | 10.36 | 0.0034 | 0.95 |

Correlation parameters are$L$, thickness of delocalized state, $K_a$, adsorption rate constant in delocalized state, $k_c$, inclusion rate constant, $D_a$, apparent diffusion coefficient.
[a]Structures based on Table 1 and DSC, Raman and gas adsorption experiments of this work: HS-I: hexagonal structure-I, TS-I: tetragonal structure-I, SCS-I: superlattice of cubic structure-I.

gas-adsorbed inner core. Fitting parameters in this model are $L$, $K_a$, $k_c$, and $D_a$. The $L$ and $K_a$ are the thickness of the delocalized adsorbed shell and the gas adsorption rate constant in the delocalized adsorbed shell, respectively. The $k_c$ is the inclusion rate constant at the interface of the gas nonincluded solid core and the $D_a$ is the apparent diffusion coefficient. The experimental data were correlated with the model in such a way that the average deviation was minimized as

$$\mathrm{AD}=\frac{10^6}{N_{\mathrm{data}}}\sum_{i=1}^{N_{\mathrm{data}}}\left|n_{\mathrm{gas,exp}}(i)-n_{\mathrm{gas,calc}}(i)\right| \tag{15}$$

where $N_{\mathrm{data}}$ is the number of data points.

Figure 2 shows correlation results for $H_2$ and $CO_2$ adsorption in semi-clathrate hydrate particles with the MAR model (Table 3, $H_2$: runs 1, 2, 5, 8, 10, $CO_2$: runs 11–15). Table 4 summarizes fitting parameters and average relative deviation (ARD) of the model, where ARD is defined as

$$\mathrm{ARD\%}=\frac{100}{N_{\mathrm{data}}}\sum_{i=1}^{N_{\mathrm{data}}}\left|\frac{n_{\mathrm{gas,exp}}(i)-n_{\mathrm{gas,calc}}(i)}{n_{\mathrm{gas,exp}}(i)}\right| \tag{16}$$

As shown in Figure 2 and Table 4, the MAR model could describe the gas adsorption process for both $CO_2$ and $H_2$ within an ARD that was generally $<3\%$.

The $L$ in the MAR model is the thickness of the delocalized gas-adsorbed outer shell, which is related to the area of the crystal grain boundary. Clathrate hydrate particles for which $L$ is large have many cracks and pores. For the TS-I structure, the $L$ values ($H_2$ systems: runs 2, 5, and 8, $CO_2$ systems: Runs 12–14 in Table 4) were in order of (high to low) TBAF, TBAB, and TBAC, and thus, this implies that the area of the crystal grain boundary was in order of (high to low) TBAF, TBAB, and TBAC. The adsorption rate constants $K_a$ for the $CO_2$ systems (3.4–35 $\times 10^{-4}$ s$^{-1}$; runs 11–15 in Table 4) had a trend of being larger than those for the $H_2$ systems (2.6–9.1 $\times 10^{-4}$ s$^{-1}$; runs 1, 2 5, 8, and 10 in Table 4), which means that the stable gas in the S-cage is rapidly adsorbed from the vapor phase. In contrast, the inclusion rate constant $k_c$ for $H_2$ systems (11–88 $\times 10^{-9}$ m·s$^{-1}$; runs 1, 2 5, 8, and 10 in Table 4) were larger than those for $CO_2$ systems (0.7–10 $\times 10^{-9}$ m·s$^{-1}$; runs 11–15 in Table 4). On the interface of the nonincluded gas solid core, the gas is included from the gas-included shell. Thus, the stable gas in the S-cage has difficulty to transfer from the gas included shell to the nonincluded gas solid core. In the gas included shell, a gas molecule diffuses through an empty S-cage or grain boundary. The diffusion coefficients $D_a$ for $H_2$ systems (1.9–20 $\times 10^{-13}$ m$^2$·s$^{-1}$; runs 1, 2 5, 8, and 10 in Table 4) were larger than those for $CO_2$ systems (0.3–2.4 $\times 10^{-15}$ m$^2$·s$^{-1}$; runs 11–15 in Table 4) as should be expected, because the molecular size of $CO_2$ is much larger than that of $H_2$. Thus, the MAR model provides trends in accordance with general physics.

In $H_2$ systems, the $K_a$, $k_c$ for TS-I structure were in order of (high to low) TBAC, TBAB, and TBAF (runs 5, 2, and 8) in Table 4, which corresponds to descending order of the lattice constant or S-cage size (TBAC, TBAB, and TBAF) in Table 1. This dependence for the S-cage size was observed for $H_2$-additive binary clathrate hydrates[39] and means that $H_2$ molecules were included in the S-cage of semi-clathrate hydrates without translation of water molecules as for $H_2$-additive binary clathrate hydrates.[39] The cause of this is thought to be that $H_2$ adsorption is difficult to be inhibited by the QAS anion due to the small molecular size of $H_2$. The $D_a$ for TS-I structures were in order of (high to low) TBAF, TBAB, and TBAC (runs 8, 5, and 2) in Table 4, which corresponds to ascending order of the area of the crystal grain boundary inferred from the relative values of $L$. Thus $H_2$ molecules probably diffuse through the grain boundaries of semi-clathrate hydrate particles.

In $CO_2$ systems, the $k_c$ for TS-I structure were in order of (high to low) TBAC, TBAB, and TBAF (Table 4, runs 12–14) and these had similar trends for $k_c$ in $H_2$ systems (Table 4, runs 2, 5, and 8). However, the $K_a$ for TS-I structure were in order of (high to low) TBAF, TBAB, and TBAC in contrast to $H_2$ systems, which corresponds to ascending order of the area of the crystal grain boundary. Thus, the $K_a$ in $CO_2$ systems were strongly influenced by the diffusivity of $CO_2$. The $D_a$ for the TS-I structure were in order of (high to low) TBAF, TBAC, and TBAB, which corresponds to ascending order of the ionic radii of the anions. From these results it can be concluded that the diffusion of $CO_2$ molecules was

**Table 5. Relationship Between Tetra-*n*-Butyl Ammonium (TBA) Salts and Clathrate Structures and Fitting Parameters, $K_a$: Adsorption Rate Constant in Delocalized State, $k_c$: Inclusion Rate Constant, $D_a$: Apparent Diffusion Coefficient**

| Parameter | Order according to structure[a] | Characteristic or Property | Relationship[b] |
|---|---|---|---|
| $H_2$ systems | | | |
| $K_a$ | TBAC > TBAB > TBAF | S-cage size | P |
| | HS-I > TS-I, SCS-I > TS-I | Distortion of hydrate cage | P |
| $k_c$ | TBAC > TBAB > TBAF | S-cage size | P |
| | SCS-I > TS-I > HS-I | Number density of S-cage | InvP |
| $D_a$ | TBAF > TBAB > TBAC | Area of crystal grain boundary | P |
| | HS-I > TS-I > SCS-I | Number density of S-cage | P |
| $CO_2$ systems | | | |
| $K_a$ | TBAF > TBAB > TBAC | Area of crystal grain boundary | P |
| | HS-I > TS-I > SCS-I | Area of crystal grain boundary | P |
| $k_c$ | TBAC > TBAB > TBAF | S-cage size | P |
| | SCS-I > TS-I > HS-I | Number density of S-cage | InvP |
| $D_a$ | TBAF > TBAC > TBAB | Ionic radius of anion | InvP |
| | HS-I > TS-I > SCS-I | Number density of S-cage | P |
| | | Number density of anion | InvP |

[a]Structure: HS-I: hexagonal structure-I, TS-I: tetragonal structure-I, SCS-I: superlattice of cubic structure-I.
[b]Relationship of parameter to characteristic: P, proportional; InvP, inversely proportional.

physically inhibited due to the S-cage by the anion, and that the relationship between the size of the gas molecule and the distorted S-cage is important for this inhibition effect.

Table 5 summarizes the many relationships between TBA salt and structure on fitting parameters ($K_a$, $k_c$, and $D_a$). According to fitting of the MAR model to the data, fitting parameters were found to be proportional or inversely proportional to the characteristics or property of the semi-clathrate hydrate (Table 5).

The effect of semi-clathrate hydrate structure on $K_a$, $k_c$, and $D_a$ is best discussed for a given TBA salt semi-clathrate hydrate. Specifically, TS-I structures are compared with HS-I structures for TBAB systems, and TS-I structures are compared with SCS-I structures for TBAF systems. However, HS-I structures cannot be compared directly with the SCS-I structures due to the lack of the common TBA salt semi-clathrate hydrate. In $H_2$ systems, $K_a$ for the TS-I structure were larger than those values for the HS-I structure (Table 4, runs 1 and 2) and for the SCS-I structure (Table 4, runs 8 and 10). It is probable that lattice defects of the semi-clathrate hydrate HS-I and SCS-I structures were larger than those for the TS-I structure. For the HS-I structure, other crystals such as ice formed in the formation process (Supporting Information Figure S1a). Water molecules in the HS-I structure are affected by that of ice, so that lattice defects in the HS-I structure occur. For the SCS-I structure, the number of anions as host molecules seems to be related to the distortion of the hydrate cages. The lattice defect of semi-clathrate hydrate cages are probably distorted by the ionic size and attracted $H_2O$ molecules to the anion as host molecule. The number of the anions as host molecules for the SCS-I structure was largest among those structures (Table 1). Thus, the number of the distorted S-cages for the SCS-I structure was probably more than that for the TS-I structure. The $k_c$ for each structure were in order of (high to low) SCS-I, TS-I, and HS-I, which corresponds to ascending order for the number of S-cages per ideal number of water molecules of the unit cell (Table 1). Conversely, the $D_a$ for each structure were in order of (high to low) HS-I, TS-I, and SCS-I, which corresponds to descending order for the number of S-cages per ideal number of water molecules of unit cell (Table 1). The relationship between the $k_c$, the $D_a$, and the number density of S-cages of the semi-clathrate hydrates exhibited similar dependencies with occupancy of the S-cage as that observed for $H_2$-THF clathrate hydrates.[49] Therefore, it can be implied that the $H_2$ adsorption rate is faster as the number density of sorbable sites decreases.

In $CO_2$ systems, the $K_a$ for each structure were in order of (high to low) HS-I, TS-I, and SCS-I, which corresponds to descending order of the $L$ parameter that is related to the area of the crystal grain boundary (Table 4, runs 11, 12, 14, and 15) as well as the anions (Table 4, runs 12–14). The $k_c$ for each structure were in order of (high to low) SCS-I, TS-I, and HS-I, and the $D_a$ for each structure were in order of (high to low) HS-I, TS-I, and SCS-I as with $H_2$ systems. Therefore, the relationship between $CO_2$ adsorption or diffusion rate and the number density of sorbable sites are the same as that for $H_2$ systems. In $CO_2$ systems, the descending order of the $D_a$ for each structure corresponds to the ascending order of the number density of the anions in semi-clathrate hydrates, because the diffusion of $CO_2$ molecules is inhibited by the distorted S-cage near the anion as a host molecule.

Table 4 summarizes fitting parameters and ARDs for $H_2$ adsorption with TBAC semi-clathrate hydrate particles (runs 3–6) and Supporting Information Figure S4 shows correlation with the MAR model. The $K_a$ for each TBAC concentration were in order of (high to low) 2.6, 3.0, 3.2, and 3.7 mol%, which shows that the nonincluded TBAC inhibited $H_2$ adsorption and diffusion. The $k_c$ for each TBAC concentration were in order of (high to low) 2.6, 3.7, 3.0, and 3.2 mol%, which means that ice was present and that TBAC probably deformed the S-cages in the TS-I structure, as $k_c$ is related to the distortion of the S-cage as well as the structure dependence in $H_2$ systems. The $D_a$ for each TBAC concentration were in order of (high to low) 3.0, 2.6, 3.7, and 3.2 mol%, which corresponds to the descending order of the $L$ as well as the anion dependency of $D_a$ and $L$ for TS-I structure in $H_2$ systems. This implies that the ice and the nonincluded TBAC not only increased the area of the crystal grain boundary but also that the ice and the nonincluded TBAC caused large resistance to $H_2$ diffusion.

### *Measurement and simulation of $H_2/CO_2$ selectivity*

Mixture gas ($H_2$ and $CO_2$) adsorption behavior was simulated using the correlated values from the gas adsorption

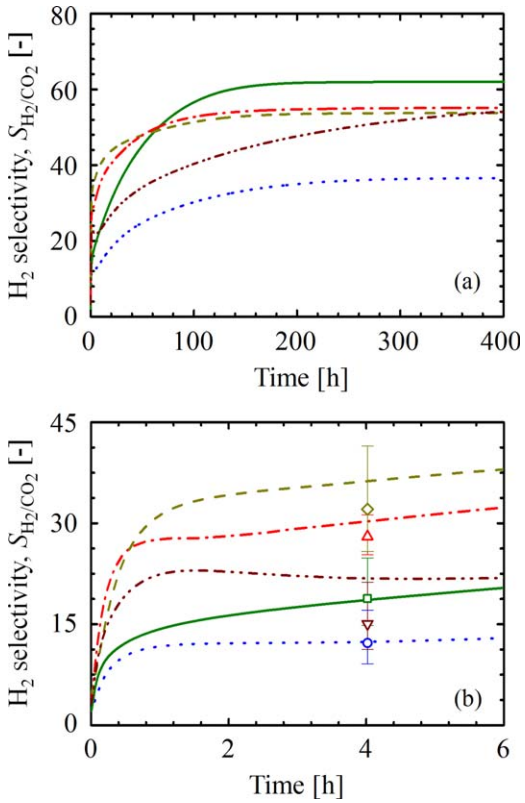


**Figure 3. $H_2$ selectivity for $CO_2$ as a function of time in the semi-clathrate hydrate particles ($d_p = 128$ μm, $T = 269$ K, $P_{initial}$ ($H_2/CO_2 = 3.4$) = 4.5 MPa).**

**(a) long time-scale and (b) short time-scale. Lines show the simulation results with the MAR model.[39] Symbols show TBA salt and structure of semi-clathrate hydrate. Symbols: red up-pointing triangle (dashed-dotted line), 2.6 mol% TBAB (HS-I); blue circle (dotted line), 3.7 mol% TBAB (TS-I); green square (continuous line), 3.2 mol% TBAC (TS-I); olive diamond (dashed line), 3.0 mol% TBAF (TS-I); brown down-pointing triangle (dashed-two dotted line), 3.3 mol% TBAF (SCS-I). Langmuir constants and fitting parameters of MAR model for each gas and semi-clathrate hydrate are given in Tables 4 and 5. [Color figure can be viewed in the online issue, which is available at wileyonlinelibrary.com.]**

measurements with MAR model to estimate $H_2/CO_2$ selectivities. The conditions of the simulation were assumed to be those of the experimental conditions as summarized in Table 2 (runs 16–20). The Langmuir constant and the parameters for MAR model in Tables 3 and 4 were used (runs 1, 2, 5, 8, and 10–15). The parameter $L$ is the semi-clathrate hydrate particle property, thus, the $L$ values used for mixture gas adsorption simulation were same as those used at $CO_2$ adsorption experiments because the particle diameters for the mixture gas adsorption experiments were the same as those in the $CO_2$ adsorption experiments.

Figure 3 shows experimental and calculated $H_2/CO_2$ selectivities for TBA salt semi-clathrate hydrates. In the simulation results, the equilibrium $H_2/CO_2$ selectivities $S_{H_2/CO_2}$ for the semi-clathrate hydrates were in order of (high to low) 3.2 mol% TBAC, 2.6 mol% TBAB, 3.3 mol% TBAF semi-clathrate hydrate, 3.0 mol% TBAF, and 3.7 mol% TBAB. The $H_2/CO_2$ selectivity for 3.2 mol% TBAC semi-clathrate hydrate was highest among the semi-clathrate hydrates. The $S_{H_2/CO_2}$ in each semi-clathrate hydrate were higher than the $S_{H_2/CO_2}$ by gas clathrate hydrate formation without additive guest molecules ($T = 273$ K, $P_{initial} = 3.8$ MPa, $n_{H_2}/n_{CO_2} = 1.6$).[17]

The rate of increase in the $S_{H_2/CO_2}$ at the early stages of adsorption were in order of (high to low) 3.0 mol% TBAF, 2.6 mol%, 3.3 mol% TBAF, 3.2 mol% TBAC, and 3.7 mol% TBAB semi-clathrate hydrate according to the simulation. In the experimental results (points in Figure 3b), the $H_2/CO_2$ selectivities $S_{H_2/CO_2}$ for the semi-clathrate hydrates at 4 h were in order of (high to low) 3.0 mol% TBAF (run 19), 2.6 mol% TBAB (run 16), 3.2 mol% TBAC semi-clathrate hydrate (run 18), 3.3 mol% TBAF (run 20), and 3.7 mol% TBAB (run 17). The $S_{H_2/CO_2}$ of the simulation results were close to those of the experimental results as shown in Figure 3b. Therefore, 3.0 mol% TBAF semi-clathrate hydrate is considered to be applicable as separation media for $H_2/CO_2$ systems in PSA processes. Because the cycle time of the gas adsorption and desorption is generally on the order of minutes, high selectivity at short contact times is required. In this section, the structure of semi-clathrate hydrates as separation media has been unified as much as possible. However, as the gas adsorption rate increases with increasing area of crystal grain boundaries, it would seem to be possible to mix other crystals, such as TBAC semi-clathrate hydrates to create more favorable systems (Supporting Information Figure S4). The gas selectivity and adsorption rate of semi-clathrate hydrates may be improved by combining semi-clathrate hydrates with additive salts and considering the structures.

### *Simulation of $H_2/CO_2$ selectivity with hydrate membrane*

Theoretical selectivity with polymeric membranes to separate a gas mixture can be calculated from the solubility and diffusivity of the species.[50] The theoretical selectivity $\alpha_{H_2/CO_2}$ of a membrane can be calculated from Eq. 17 as

$$\alpha_{H_2/CO_2} = \frac{p_{H_2}}{p_{CO_2}} = \frac{C_{H_2,S}}{C_{CO_2,S}} \frac{D_{H_2}}{D_{CO_2}} \tag{17}$$

where $p$ is the species permeability. In the use of Eq. 17 for a hydrate membrane, the apparent diffusion coefficient depends on occupancy,[49] which means that the diffusion coefficient depends on the partial pressure of the gas, $P_{gas}$. Thus, the gas permeability is calculated from Eqs. 18–21 with Langmuir constants and apparent diffusion coefficients as

$$p_{gas} = \frac{d_m F_{gas}}{A_m \left(P_{gas,inlet} - P_{gas,outlet}\right)} \tag{18}$$

$$F_{gas} = D_{e,gas} A_m \frac{\left(C_{gas,m,inlet} - C_{gas,m,outlet}\right)}{d_m} \tag{19}$$

$$D_{e,gas} = \left(1 - \theta_{S,gas}\right) D_{a,gas} \tag{20}$$

$$C_{gas,m,inlet} = \frac{N_S}{N_A V_{unitcell}} \left( \frac{C_{gas,S} f_{gas,inlet}}{1 + C_{H_2,S} f_{H_2,inlet} + C_{CO_2,S} f_{CO_2,inlet}} \right) \tag{21}$$

where $A_m$, $d_m$, $F$, $C_{gas,m,inlet}$, $\theta_S$, and $C_{gas,S}$ are the membrane area, membrane thickness, gas permeate flow rate, supply side gas concentration, S-cage occupancy, and Langmuir constant for the gas in the S-cage, respectively. The effective diffusion coefficient, $D_{e,gas}$ in Eq. 20 is related to the apparent diffusion coefficient, $D_{a,gas}$ by the occupancy in the S-cage. Figure 4 shows the pressure dependence of $H_2$ and $CO_2$ permeability. As the total pressure increases, the $H_2$ and

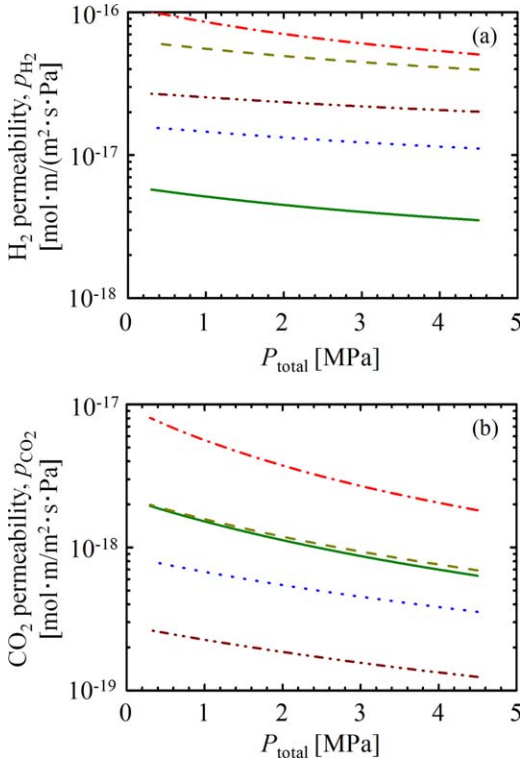


**Figure 4. Effect of pressure on gas permeability for semi-clathrate hydrate membrane at 269 K and initial $H_2/CO_2 = 3.4$.**

**(a) $H_2$ permeability and (b) $CO_2$ permeability. Lines show TBA salt and structure of semi-clathrate hydrate. Lines: red dashed-dotted line, 2.6 mol% TBAB (HS-I); blue dotted line, 3.7 mol% TBAB (TS-I); green continuous line, 3.2 mol% TBAC (TS-I); olive dashed line, 3.0 mol% TBAF (TS-I); brown dashed-two dotted line, 3.3 mol% TBAF (SCS-I). [Color figure can be viewed in the online issue, which is available at wileyonlinelibrary.com.]**

$CO_2$ permeability decreases for all semi-clathrate hydrates. As the gas partial pressure increases, the adsorption amount of the gas increases. However, as the occupancy of the gas increases, the effective diffusion coefficient decreases as Eq. 20. Therefore, the trend of gas permeability with pressure is due to the decrease in the ratio of gas diffusion rates being larger than the increase in the ratio of the gas adsorption amounts.

Figure 5 shows the pressure dependence of $H_2/CO_2$ selectivity versus $H_2$ permeability. As the $H_2$ permeability increases, $H_2/CO_2$ selectivity decreases for all semi-clathrate hydrates. The reason for this is thought to be due to the decreasing ratio of $CO_2$ permeability to $H_2$ permeability (Figure 4) for increasing pressures, as the $CO_2$ occupancy of the S-cage is higher than that of the $H_2$ occupancy. The variation of selectivity with pressure for clathrate hydrate membranes is completely different from the separation characteristics of polymeric membranes.[50] For semi-clathrate hydrate membranes, as pressure increases, $H_2/CO_2$ selectivity increases. The SCS-I structure TBAF semi-clathrate hydrate seems to be most favorable for use as a hydrate membrane among the semi-clathrate hydrates examined as it can be used at conditions close to ambient temperature. However, it is probable that gas selectivity of semi-clathrate hydrates can be made even higher for other QAS than TBAF that lower

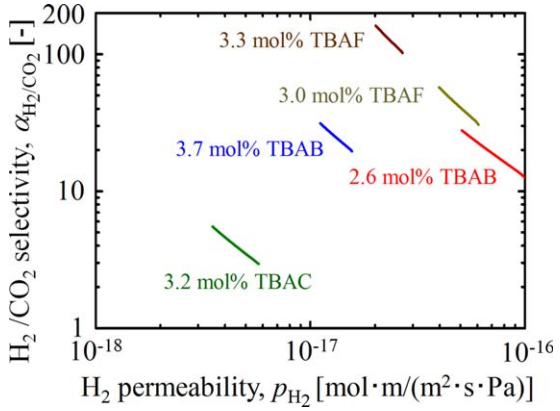


**Figure 5. Relationship between $H_2$ permeability and $H_2/CO_2$ selectivity at 269 K and initial $H_2/CO_2 = 3.4$.**

**Lines show TBA salt and structure of semi-clathrate hydrate. Lines: red, 2.6 mol% TBAB (HS-I); blue, 3.7 mol% TBAB (TS-I); green, 3.2 mol% TBAC (TS-I); olive, 3.0 mol% TBAF (TS-I); brown, 3.3 mol% TBAF (SCS-I). [Color figure can be viewed in the online issue, which is available at wileyonlinelibrary.com.]**

the permeability of large size molecules or by control of the clathrate structure. Based on the above results, the semi-clathrate hydrates examined in this work are favorable for applications in membrane separation due to their high selectivity and mild operating conditions. Further research is needed on membrane support materials for semi-clathrate hydrates and on conditions for semi-clathrate hydrate thin film formation or particle formation methods.

## Conclusions

In this work, the formation TBA salt semi-clathrate hydrate particles were analyzed by DSC, Raman spectroscopy and by consideration of the equilibrium $H_2$ storage amounts. The TBA salts used were TBAB, TBAC, and TBAF. TBAC semi-clathrate hydrate formed TS-I structure regardless of TBAC concentration and 3.2 mol% TBAC semi-clathrate hydrate formed without forming ice. TBAF semi-clathrate hydrate formed TS-I structure for 3.0 mol% TBAF and SCS-I structure for 3.3 mol% TBAF at small degrees of supercooling.

The $H_2$ or $CO_2$ adsorption rates with the semi-clathrate hydrate particles were measured with a pressure decay method. The time for half of the equilibrium consumption, $t_{half}$, strongly depended on the anion of TBA salt for $H_2$ systems, whereas $H_2$ adsorption was not a strong function of the semi-clathrate hydrate structure. The $t_{half}$ in $CO_2$ systems depended not only on the anion of the TBA salt but also on the semi-clathrate hydrate structure, and this is attributed to the size of the $CO_2$ molecule. The equilibrium $H_2$ occupancy in the S-cage $\theta_{S,H_2,eq}$ strongly depended on the semi-clathrate hydrate structure rather than on the anion of the TBA salt. The equilibrium $CO_2$ occupancy in S-cage $\theta_{S,CO_2,eq}$ depended not only on the semi-clathrate structure but also on the TBA salt for TS-I structure. The size of the distorted S-cage of TBAC semi-clathrate hydrate is optimum for $CO_2$ molecule because the $\theta_{S,CO_2,eq}$ for TBAC semi-clathrate hydrate was highest among TS-I structures.

From the results in this study, it is implied that the stable gas in the S-cage ($CO_2$) is rapidly adsorbed from the vapor

phase, as the adsorption rate constants $K_a$ of $CO_2$ were larger than those of $H_2$ for the same semi-clathrate hydrate systems. Conversely, the stable gas in the S-cage ($CO_2$) transfers with difficulty in the gas included shell as can be concluded from the simulation results, as the inclusion rate constants $k_c$ and the diffusion coefficients $D_a$ for $H_2$ systems were larger than those for $CO_2$ systems. The $k_c$ increased for both $H_2$ and $CO_2$ systems with decreasing the number density of S-cages. In contrast, the $D_a$ for both $H_2$ and $CO_2$ systems increased with increasing the number density of S-cages. Therefore, the gas inclusion rate became faster as the number density of sorbable sites decreased, and the gas diffusion rate became faster as the number density of sorbable site increased. The $D_a$ for $CO_2$ systems decreased with increasing number density of the anions. This means that the diffusion of $CO_2$ molecules was inhibited by the S-cage near the anion as host molecule.

The $H_2/CO_2$ selectivities $S_{H_2/CO_2}$ for TBA salt semi-clathrate hydrates were obtained from MAR model simulations with Langmuir constants obtained from experiments. In the simulation results, the $S_{H_2/CO_2}$ for 3.2 mol% TBAC semi-clathrate hydrate was the highest among the TBA salt semi-clathrate hydrates studied. Conversely, the $S_{H_2/CO_2}$ for 3.0 mol% TBAF semi-clathrate hydrate in the early stages of gas adsorption was the highest among the TBA salt semi-clathrate hydrates studied. The 3.0 mol% TBAF semi-clathrate hydrate is considered to be appropriate as separation media for $H_2/CO_2$ systems in PSA processes among the semi-clathrate hydrate systems studied. The $H_2/CO_2$ selectivities for semi-clathrate hydrates can probably be improved using additive salts to control the structure.

The $H_2/CO_2$ selectivities $\alpha_{H_2/CO_2}$ for TBA salt semi-clathrate hydrates were calculated from Langmuir constants and apparent diffusion coefficients. The $\alpha_{H_2/CO_2}$ for 3.3 mol% TBAF semi-clathrate hydrate was highest among the TBA salt semi-clathrate hydrates studied and had a value that was greater than 100. Thus, semi-clathrate hydrates can have wide application as separation media. For semi-clathrate hydrates, the $\alpha_{H_2/CO_2}$ increased with decreasing gas permeability. Therefore, the characteristics required for semi-clathrate hydrate membranes are different from semi-clathrate hydrate particles that might be used for a PSA process. In either separation process, however, the adsorption and diffusion characteristics of the larger molecules can be controlled by choice of the QAS and the use of conditions to form appropriate semi-clathrate hydrate structures.

## Acknowledgments

The authors are grateful for Japan Society for the Promotion of Science for partial financial support of this research through a Grant-in-Aid for Scientific Research and a doctoral course fellowship.

## Notation

$A_{GC}$ = peak area of gas chromatography (GC)
$A^*_{GC}$ = peak area given by GC analysis for the pure gas
$A_m$ = membrane area, $m^2$
AD = average deviation, mol
ARD = average relative deviation, %
$a, b, c$ = lattice constants, Å
$C_{gas}$ = gas concentration, $mol/m^3$
$C_S$ = Langmuir constant of S-cage, $Pa^{-1}$
$C^*_S$ = actual Langmuir constant of S-cage, $Pa^{-1}$
$D_a$ = apparent diffusion coefficient, $m^2/s$
$D_e$ = effective diffusion coefficient, $m^2/s$
$d_m$ = membrane thickness, m
$F$ = gas permeate flow rate, mol/s
$f$ = fugacity, Pa
$K_a$ = adsorption rate constant in delocalized state, $s^{-1}$
$k_c$ = inclusion rate constant on interface of $H_2$ nonincluded solid core, m/s
$L$ = thickness of delocalized gas-adsorbed outer shell, m
$M$ = molecular weight, g/mol
$N$ = number
$N_A$ = Avogadro constant, $mol^{-1}$
$N^*_{H_2O}$ = theoretical number of water molecules per unit cell
$N_{ideal,H_2O}$ = number of water molecules per unit cell of structure non-replaced $H_2O$
$N_{Occ,H_2O}$ = number of occupied water molecules in S-cage per unit cell
$n$ = mole number, mol
$P$ = pressure, Pa
$p$ = permeability, $mol \cdot m/(m^2 \cdot s \cdot Pa)$
$S_{H_2/CO_2}$ = equilibrium $H_2/CO_2$ selectivity for semi-clathrate hydrate particles
$T$ = temperature, K
$t$ = time, h
$V$ = volume, $m^3$
$X$ = storage amount with respect to the hydrates, $mmol_{gas}/mol_{H_2O+TBA\ salt}$
$y$ = composition in vapor phase

### Greek letters

$\alpha_{H_2/CO_2}$ = $H_2/CO_2$ selectivity for semi-clathrate hydrate membrane
$\Delta T$ = degree of supercooling, K
$\varepsilon$ = porosity
$\theta_S$ = occupancy in S-cage
$\theta^*_S$ = occupancy in S-cage nonoccupied with $H_2O$
$\rho$ = density, $g/m^3$

### Subscripts

Ab = grain boundary
calc = calculation
cell = hydrate formation cell
$CO_2$ = carbon dioxide
data = data point
eq = equilibrium state
exp = experiment
Gas = gas molecule
$H_2$ = hydrogen
$H_2O$ = water
half = consumption of half of gas
Hyd = hydrate phase
inlet = supply side
load = loading
m = membrane
other = other guest molecule
outlet = permeation side
R, initial = before loading of reservoir tank
R, final = after loading of reservoir tank
S = S-cage
TBAB = tetra-*n*-butyl ammonium bromide
TBAC = tetra-*n*-butyl ammonium chloride
TBAF = tetra-*n*-butyl ammonium fluoride
TBA salt = tetra-*n*-butyl ammonium salt
Theor Hyd = theoretical hydrate
vapor = vapor phase
leak = leak of gas molecule

## Literature Cited

1. Alarcon-Rodriguez A, Ault G, Galloway S. Multi-objective planning of distributed energy resources: a review of the state-of-the-art. *Renew Sustain Energy Rev*. 2010;14:1353–1366.
2. Mohammed YS, Mustafa MW, Bashir N, Mokhtar AS. Renewable energy resources for distributed power generation in Nigeria: a review of the potential. *Renew Sustain Energy Rev*. 2013;22:257–268.
3. Alfonso D, Perpina C, Perez-Navarro A, Penalvo E, Vargas C, Cardenas R. Methodology for optimization of distributed biomass resources evaluation, management and final energy use. *Biomass Bioenergy*. 2009;33:1070–1079.
4. Perpina C, Alfonso D, Perez-Navarro A, Penalvo E, Vargas C, Cardenas R. Methodology based on geographic information systems

for biomass logistics and transport optimisation. *Renew Energy*. 2009;34:555–565.
5. Alonso-Vicario A, Ochoa-Gomez JR, Gil-Rio S, Gomez-Jimenez-Aberasturi O, Ramirez-Lopez CA, Torrecilla-Soria J, Dominguez A. Purification and upgrading of biogas by pressure swing adsorption on synthetic and natural zeolites. *Microporous Mesoporous Mater*. 2010;134:100–107.
6. Ryckebosch E, Drouillon M, Veruaeren H. Techniques for transformation of biogas to biomethane. *Biomass Bioenergy*. 2011;35:1633–1645.
7. Bauer F, Persson T, Hulteberg C, Tamm D. Biogas upgrading—technology overview, comparison and perspectives for the future. *Biofuels Bioprod Biorefining*. 2013;7:499–511.
8. Onstot WJ, Minet RG, Tsotsis TT. Design aspects of membrane reactors for dry reforming of methane for the production of hydrogen. *Ind Eng Chem Res*. 2001;40:242–251.
9. Fermoso J, He L, Chen D. Sorption enhanced steam reforming (SESR): a direct route towards efficient hydrogen production from biomass-derived compounds. *J Chem Technol Biotechnol*. 2012;87:1367–1374.
10. Aaron D, Tsouris C. Separation of $CO_2$ from flue gas: a review. *Sep Sci Technol*. 2005;40:321–348.
11. Simo M, Sivashanmugam S, Brown CJ, Hlavacek V. Adsorption/desorption of water and ethanol on 3A zeolite in near-adiabatic fixed bed. *Ind Eng Chem Res*. 2009;48:9247–9260.
12. Kang SP, Lee H. Recovery of $CO_2$ from flue gas using gas hydrate: thermodynamic verification through phase equilibrium measurements. *Environ Sci Technol*. 2000;34:4397–4400.
13. Shimada W, Ebinuma T, Oyama H, Kamata Y, Takeya S, Uchida T, Nagao J, Narita H. Separation of gas molecule using tetra-*n*-butyl ammonium bromide semi-clathrate hydrate crystals. *Jpn J Appl Phys Part 2*. 2003;42:L129–L131.
14. Seo YT, Moudrakovski IL, Ripmeester JA, Lee JW, Lee H. Efficient recovery of $CO_2$ from flue gas by clathrate hydrate formation in porous silica gels. *Environ Sci Technol*. 2005;39:2315–2319.
15. Kamata Y, Yamakoshi Y, Ebinuma T, Oyama H, Shimada W, Narita H. Hydrogen sulfide separation using tetra-n-butyl ammonium bromide semi-clathrate (TBAB) hydrate. *Energy Fuels*. 2005;19:1717–1722.
16. Duc NH, Chauvy F, Herri JM. $CO_2$ capture by hydrate crystallization—a potential solution for gas emission of steelmaking industry. *Energy Convers Manag*. 2007;48:1313–1322.
17. Kumar R, Linga P, Ripmeester JA, Englezos P. Two-stage clathrate hydrate/membrane process for precombustion capture of carbon dioxide and hydrogen. *J Environ Eng-ASCE*. 2009;135:411–417.
18. Zhong DL, Ye Y, Yang C, Bian Y, Ding K. Experimental investigation of methane separation from low-concentration coal mine gas ($CH_4/N_2/O_2$) by tetra-*n*-butyl ammonium bromide semiclathrate hydrate crystallization. *Ind Eng Chem Res*. 2012;51:14806–14813.
19. Song YC, Wan XJ, Yang MJ, Jiang LL, Liu Y, Dou BL, Zhao JF, Wang SR. Study of selected factors affecting hydrate-based carbon dioxide separation from simulated fuel gas in porous media. *Energy Fuels*. 2013;27:3341–3348.
20. Linga P, Adeyemo A, Englezos P. Medium-pressure clathrate hydrate/membrane hybrid process for postcombustion capture of carbon dioxide. *Environ Sci Technol*. 2008;42:315–320.
21. Adeyemo A, Kumar R, Linga P, Ripmeester J, Englezos P. Capture of carbon dioxide from flue or fuel gas mixtures by clathrate crystallization in a silica gel column. *Int J Greenhouse Gas Control*. 2010;4:478–485.
22. Tang J, Zeng D, Wang C, Chen Y, He L, Cai N. Study on the influence of SDS and THF on hydrate-based gas separation performance. *Chem Eng Res Des*. 2013;91:1777–1782.
23. McMullan R, Jeffrey GA. Hydrates of the tetra-n-butyl and tetra-i-amyl quaternary ammonium salts. *J Chem Phys*. 1959;31:1231–1234.
24. Oyama H, Shimada W, Ebinuma T, Kamata Y, Takeya S, Uchida T, Nagao J, Narita H. Phase diagram, latent heat, and specific heat of TBAB semiclathrate hydrate crystals. *Fluid Phase Equilib*. 2005;234:131–135.
25. Davidson DW. *Water—A Comprehensive Treatise*, *vol. 2*. New York: Plenum Press, 1973.
26. Li SF, Fan SS, Wang JQ, Lang XM, Liang DQ. $CO_2$ capture from binary mixture via forming hydrate with the help of tetra-*n*-butyl ammonium bromide. *J Nat Gas Chem*. 2009;18:15–20.
27. Xu CG, Zhang SH, Cai J, Chen ZY, Li XS. $CO_2$ (carbon dioxide) separation from $CO_2$-$H_2$ (hydrogen) gas mixtures by gas hydrates in TBAB (tetra-*n*-butyl ammonium bromide) solution and Raman spectroscopic analysis. *Energy*. 2013;59:719–725.
28. Park S, Lee S, Lee Y, Seo Y. $CO_2$ capture from simulated fuel gas mixtures using semiclathrate hydrates formed by quaternary ammonium salts. *Environ Sci Technol*. 2013;47:7571–7577.
29. Fan SS, Li SF, Wang JQ, Lang XM, Wang YH. Efficient capture of $CO_2$ from simulated flue gas by formation of TBAB or TBAF semiclathrate hydrates. *Energy Fuels*. 2009;23:4202–4208.
30. Rodionova T, Komarov V, Villevald G, Aladko L, Karpova T, Manakov A. Calorimetric and structural studies of tetrabutylammonium chloride ionic clathrate hydrates. *J Phys Chem B*. 2010;114:11838–11846.
31. Dyadin YA, Udachin KA. Clathrate polyhydrates of peralkylonium salts and their analogs. *J Struct Chem*. 1987;28:394–432.
32. Shimada W, Shiro M, Kondo H, Takeya S, Oyama H, Ebinuma T, Narita H. Tetra-*n*-butylammonium bromide-water (1/38). *Acta Crystallogr C*. 2005;61:O65–O66.
33. Dyadin YA, Terekhova IS, Polyanskaya TM, Aladko LS. Clathrate hydrates of tetrabutylammonium fluoride and oxalate. *J Struct Chem*. 1976;17:566–571.
34. Komarov VY, Rodionova TV, Terekhova IS, Kuratieva NV. The cubic superstructure-I of tetrabutylammonium fluoride $(C_4H_9)_4NF{\cdot}29.7H_2O$ clathrate hydrate. *J Incl Phenom Macrocycl Chem*. 2007;59:11–15.
35. Muromachi S, Udachin KA, Shin K, Alavi S, Moudrakovski IL, Ohmura R, Ripmeester JA. Guest-induced symmetry lowering of an ionic clathrate material for carbon capture. *Chem Commun (Cambridge, England)*. 2014;50:11476–11479.
36. Sakamoto J, Hashimoto S, Tsuda T, Sugahara T, Inoue Y, Ohgaki K. Thermodynamic and Raman spectroscopic studies on hydrogen + tetra-*n*-butyl ammonium fluoride semi-clathrate hydrates. *Chem Eng Sci*. 2008;63:5789–5794.
37. Sizikov AA, Manakov AY, Rodionova TV. Methane capacity of double tetrabutylammonium bromide plus methane ionic clathrate hydrates. *Energy Fuels*. 2012;26:3711–3716.
38. Komatsu H, Hayasaka A, Ota M, Sato Y, Watanabe M, Smith RL. Measurement of pure hydrogen and pure carbon dioxide adsorption equilibria for THF clathrate hydrate and tetra-*n*-butyl ammonium bromide semi-clathrate hydrate. *Fluid Phase Equilib*. 2013;357:80–85.
39. Komatsu H, Ota M, Sato Y, Watanabe M, Smith RL. Multiple adsorption resistance model for constituent molecular effects of hydrogen clathration-kinetics in clathrate hydrate particles. *Chem Eng Sci*. 2014;108:270–282.
40. Sloan ED, Koh CA. *Clathrate Hydrates of Natural Gases*, 3rd ed. Boca Raton: CRC Press, 2007.
41. NIST Chemistry WebBook. Available at http://webbook.nist.gov/chemistry/. Accessed March, 2013.
42. Spano JO, Heck CK, Barrick PL. Liquid-vapor equilibria of hydrogen-carbon dioxide system. *J Chem Eng Data*. 1968;13:168–171.
43. Yorizane M, Yoshimura S, Masuoka H. Vapor liquid equilibrium at high pressure ($N_2$-$CO_2$, $H_2$-$CO_2$ system). *Kagaku Kogaku*. 1970;34:953–957.
44. Tsang CY, Streett WB. Phase equilibria in the $H_2/CO_2$ system at temperatures from 220 K to 290 K and pressures to 172 MPa. *Chem Eng Sci*. 1981;36:993–1000.
45. Bezanehtak K, Combes GB, Dehghani F, Foster NR, Tomasko DL. Vapor-liquid equilibrium for binary systems of carbon dioxide plus methanol, hydrogen plus methanol, and hydrogen plus carbon dioxide at high pressures. *J Chem Eng Data*. 2002;47:161–168.
46. Staykova DK, Kuhs WF, Salamatin AN, Hansen T. Formation of porous gas hydrates from ice powders: diffraction experiments and multistage model. *J Phys Chem B*. 2003;107:10299–10311.
47. Joung IS, Cheatham TE. Determination of alkali and halide monovalent ion parameters for use in explicitly solvated biomolecular simulations. *J Phys Chem B*. 2008;112:9020–9041.
48. Sloan ED. Fundamental principles and applications of natural gas hydrates. *Nature*. 2003;426:353–359.
49. Hashimoto S, Yamamoto K, Tsuda T, Inoue Y. Modeling on hydrogen absorption in tetrahydrofuran hydrate. *J Chem Eng Jpn*. 2012;45:444–451.
50. Lin HQ, Van Wagner E, Freeman BD, Toy LG, Gupta RP. Plasticization-enhanced hydrogen purification using polymeric membranes. *Science*. 2006;311:639–642.

*Manuscript received Feb. 16, 2014, and revision received Oct. 12, 2014.*